Available online at www.sciencedirect.com

ScienceDirect

Procedia Engineering 101 (2015) 322 – 329

Procedia Engineering

www.elsevier.com/locate/procedia

3rd International Conference on Material and Component Performance under Variable Amplitude Loading, VAL2015

Investigation of variable amplitude loading and stress ratio in the very high cycle fatigue regime using micro-notched specimens

Thomas Müller*, Manuela Sander

Institute of Structural Mechanics (StM), University of Rostock, Albert-Einstein-Str. , D-18059 Rostock, Germany

Abstract]

In order to study the effect of small defects in the regime of very high cycle fatigue, 20 µm deep micro-notches are introduced into the specimens by laser sublimation. Tests are performed using an ultrasonic fatigue testing system. For the variable amplitude loading tests a reconstructed load sequence on the basis of a standardized load time history called FELIX is used and transformed to the stress ratios of -1 and 0. The experimental results are compared to previous investigations with smooth specimens. Moreover, calculated Gassner lines using the linear damage accumulation are compared to the experimental results.

Peer-review under responsibility of the Czech Society for Mechanics

Keywords: very high cycle fatigue, reconstructed load spectrum, micro-notches, linear damage accumulation

1. Introduction

Since modern components in service, like wheelset axles or helicopter rotors, have to endure increasingly fatigue lives, investigations in the very high cycle fatigue (VHCF) regime ($N > 10^7$ cycles) attract growing importance. For cyclic stress amplitudes below the fatigue strength a decrease of the S-N curve is observed in the range of VHCF, due to the transition from surface to subsurface crack initiation. At high strength steels the crack initiates generally at non-metallic inclusions with a typical fish-eye formation.

Despite a few authors, e.g. [1-5], the influence of variable amplitude (VA) loadings in the VHCF has previously been barely investigated. Two block loading tests with 0.15% C steel performed by *Mayer* et al. [1] show that lower

* Corresponding author. Tel.: +49 381 498 9345; fax: +49 381 498 3942.
E-mail address: thomas.mueller@uni-rostock.de

Peer-review under responsibility of the Czech Society for Mechanics
doi:10.1016/j.proeng.2015.02.039

stress amplitudes beneath the fatigue strength have only a damaging effect, if the higher stress amplitudes are more than 15% of the fatigue strength. But, they do not contribute to the damage, if the higher stress amplitude is lower than 15% of the fatigue strength. This phenomenon can also be observed by *Müller* and *Sander* [2] in two block loading tests for 34CrNiMo6. Moreover, the ratio between the number of cycles of low and high load amplitude influences the fatigue life, depending on the ratio between high and low stress amplitudes. Variable amplitude loading tests with differently reconstructed load time histories were performed by *Müller* and *Sander* [5]. Furthermore, a new modified linear damage calculation approach considering inclusion sizes has been developed and validated with the experimental results.

However, in service, components are exposed environmental conditions like corrosion or stone chipping that can induce small-scaled defects on the components surface and, as a consequence of this, can provoke surface crack initiation. The tolerable cyclic loading in the case of those defects, like corrosion pits, can be evaluated by linear fracture mechanics, as it was done by several authors, e.g. [6-8]. It is assumed that small surface defects can be treated as effective cracks. *Masaki* et al. [6] observed a reduction in the fatigue strength and an increasing number of fatigue failures in the VHCF regime of specimens with 0.5 mm large artificial corrosion pits in comparison to smooth specimen. Furthermore, non-propagating cracks occurred at the bottom of the corrosion pits. Investigations with pitted 12% Cr steam turbine blade steel [7] showed a significant influence of the environmental conditions on the fatigue life.

In this investigation, fatigue tests with constant and variable amplitude loadings with micro-notched specimens are performed using an ultrasonic fatigue testing system. The experimental results are compared to tests with inclusion induced fatigue failure of smooth specimen. Furthermore, crack initiation is evaluated using approaches based on the linear fracture mechanics. Different linear damage accumulations, which considerate load amplitudes beneath the fatigue strength not equally, are used to calculate the fatigue life and to evaluate the influence of lower load amplitudes in the VHCF.

Nomenclature

a_0	*El Haddad* parameter
area	area of defect (micro-notch, inclusion)
f_1, f_2	factor for stress intensity factor and threshold stress solution by *Murakami*
HV	*Vicker's* hardness
R	stress ratio
ΔK_{defect}, $\Delta K_{defect,eq}$	stress intensity factor range of the defect for constant and variable amplitude loading
$\Delta K_{th,long}$, $\Delta K_{th,sc}$	threshold stress intensity factor for long cracks and short crack
$\Delta\sigma_D$	fatigue strength range
σ_a, $\bar{\sigma}_a$	stress amplitude and maximum stress amplitude of load sequence
σ_w	threshold stress by *Murakami*

2. Threshold approaches based on fracture mechanics

There are different approaches based on fracture mechanics considering small surface and subsurface defects as equivalent cracks. *Murakami* [10] introduce the well-known √area-approach to calculate a threshold stress intensity factor (SIF)

$$K_{th,sc} = 3.3 \cdot 10^{-3} \cdot (HV + 120) \cdot \left(\sqrt{area}\right)^{1/3} \tag{1}$$

for short cracks depending on the crack size and the hardness of the material.

Furthermore, using the definition of the maximum SIF

$$K_{max} = f_1 \cdot \sigma_o \sqrt{\pi \cdot \sqrt{area}} \tag{2}$$

with $f_1 = 0.5$ for internal defects and $f_1 = 0.65$ for surface defects as well as the equation (1) a threshold stress can be calculated

$$\sigma_w = \frac{f_2 \cdot (HV + 120)}{\left(\sqrt{area}\right)^{1/6}} \left[\frac{1-R}{2}\right]^{\alpha} \tag{3}$$

for subsurface defects (f_2=1.56) and surface defect (f_2=1.43), with the experimentally determined parameter $\alpha = 0.522$.

Fujimoto et al. [11] use the concept of the inherent damage zone and proposes an alternative formulation for the threshold stress intensity factor

$$\Delta K_{th,sc} = \frac{\sqrt{\pi \cdot a \cdot r_0 (2a + r_0)}}{(a + r_0)} \Delta\sigma_D \tag{4}$$

with $r_0 = a_0/2$. a_0 is the *El Haddad* parameter depending on the threshold stress intensity for long cracks and the fatigue strength.

3. Material and experimental procedure

Fatigue tests are performed with the quenched and tempered high-strength steel 34CrNiMo6 (see table 1 and 2). Hourglass specimens with a minimum diameter of 4 mm were machined from a 20 mm round bar. The average *Vicker's* hardness of the material is 350 HV. The surface of the specimen has been emery-polished after machining.

Table 1: Chemical composition of 34CrNiMo6 (in wt %)

C	Si	Mn	Cr	Mo	Ni
0.34	0.3	0.5	1.5	0.2	1.5

Table 2: Mechanical properties

R_m [MPa]	R_e [MPa]	E-Modulus [GPa]	A_5 [%]
1200	1000	210	9

The micro-notches are introduced by laser sublimation technique using a pico-second laser. The notches are situated at the middle of the gauge length of the specimen. Measurements with a laser confocal microscope reveal a length of 40 µm perpendiculars to the length direction of the specimen, a width of 20 µm and a depth about 20 µm. Afterwards, the specimens were annealed at 500 °C for one hour to reduce residual stresses.

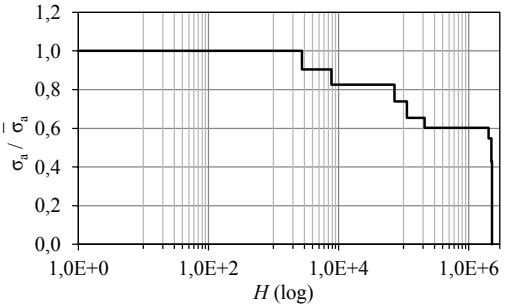

Fig. 1: Normalized reconstructed load time history FELIX [9]

Table 3: VA-Tests

Reconstructed load time history	R	$\bar{\sigma}_a$ [MPa]	Amount of cycles above fatigue strength
FELIX	-1	776	9.2%
		705	5.0%
		673	3.2%
		641	3.2%
	0	465	9.2%
		444	5.0%
		423	3.2%

The central unit of the experimental setup is an ultrasonic testing system with a testing frequency of 21 kHz developed by the BOKU Vienna. The vibration leads to a cyclic strain in the central region of the specimen, while both ends oscillate in opposite direction. This testing system is extended with a computer-controlled load frame in order to perform experiments with different mean stresses [4]. The ultrasonic testing system as well as the load frame is controlled by the software Ultrasonic Fatigue Testing Software for Variable Amplitude Loading (UFaTeS^{VAL}),

which has been developed at the Institute of Structural Mechanics at the University of Rostock [2] and is used for both the measuring data logging and controlling of the experiments.

The stress amplitude is subjected in a pulsed mode to avoid excessive heating of the specimen. Furthermore, VA-tests are performed in terms of block loadings due to increasing and decreasing stress amplitudes at the beginning and at the end of the pulse with a minimum pulse length of about 50 ms

For the experimental investigations of the VA loading the standardized helicopter load spectrum FELIX has been used. Therefore, the stress amplitudes of the FELIX spectrum have been transformed to the constant *R*-ratios of -1 and 0 using the equations accounting for the mean stress effect. The value for the mean stress effect has been experimentally determined for the VHCF [4]. This spectrum has been divided into different classes considering the requirements of the ultrasonic testing. Figure 1 shows the normalized frequency distribution of the modified FELIX spectrum [9]. The classes have been reconstructed to a load sequence starting with the highest and ending with the lowest load amplitude. The spectrum has been scaled with different maximum load amplitudes that most of the amplitudes of the spectrum are below the fatigue strength, Table 1. This sequence is repeated until the specimen fails or the limit of 10^9 cycles is reached.

4. Experimental results

4.1. Fatigue behavior for constant amplitude loading

In previous investigations [4-5] it has been shown that non-metallic inclusions lead to fatigue failure in the VHCF regime for smooth specimens. Thereby, predominantly subsurface inclusions lead to crack initiation with the typical fish-eye fracture. However, a few inclusions situated at the surface can also lead to crack initiation.

In this investigation the fatigue behavior of micro-notches with a size of the smallest observed surface inclusion of a √area of about 35 µm are compared to fatigue results of the subsurface inclusions (SSI) and surface inclusions (SI).

The results of CA tests with both stress ratios R = [-1; 0] using smooth and micro-notched specimen are shown in Figure 2. The modified S-N curve (Figure 2a) using the √*area* approach (Eq. (3)) shows a decrease of the normalized stress amplitude σ_a/σ_w with increasing fatigue life N_f for the SI and SSI results for both *R*-ratios. For R = -1 and micro-notches, the results are in good agreement with the results of SI. In contrast, for R = 0 the results tends to lower fatigue lives compared to SI results. However, run-outs of micro-notched specimen are above the calculated threshold stress amplitude σ_w for both R-ratios, because the σ_a/σ_w - values are greater one. In comparison to the SI and SSI results, micro-notches lead to no VHCF failure and it can be observed a sharp transition from failure to the fatigue strength regime.

For R = -1 the largest defect size, which leads to fatigue failure, can be observed at subsurface inclusions, as shown in Figure 2b. Crack initiation at surface inclusions occurs even at smaller defect sizes compared to SSIs. Moreover, subsurface inclusions sizes are always larger than the size of the micro-notch. The fatigue life for SI and micro-notches are the same, if the defect size is the same. As opposed to this, for R = 0 SSI sizes in the range of the micro-notch and even smaller lead to fatigue failure in the VHCF regime.

The cyclic stress intensity factor ΔK_{defect} of the defect using equation (2) as a function of the fatigue life, shown in Figure 2c, lead to values beneath the threshold value $\Delta K_{th,long\ (R = -1)}$ for long cracks for R = -1. However, for R = 0, ΔK_{defect} values are above the threshold value $\Delta K_{th,long\ (R = 0)}$ for long cracks for some inclusions.

Thus, the threshold value for long crack is not suitable as crack initiation threshold value in the range of the micro notch size. In order to fit the results more suitable, the defect size has to be considered. Therefore, the threshold stress intensity factors ΔK_{th} as a function of the defect size by *Murakami* (Eq. (1)) and *Fujimoto* (Eq. (4)) are compared with the calculated stress intensity factors ΔK_{defect} of the experimental results of micro-notches for both R-ratios, as shown in Figure 4a. For $\Delta K_{defect}/\Delta K_{th} > 1$ the stress intensity range of the defect is higher than the threshold stress intensity range and a crack should initiate, if the approach predicts the mechanism correctly. For $\Delta K_{defect}/\Delta K_{th} < 1$ no crack initiation should occur.

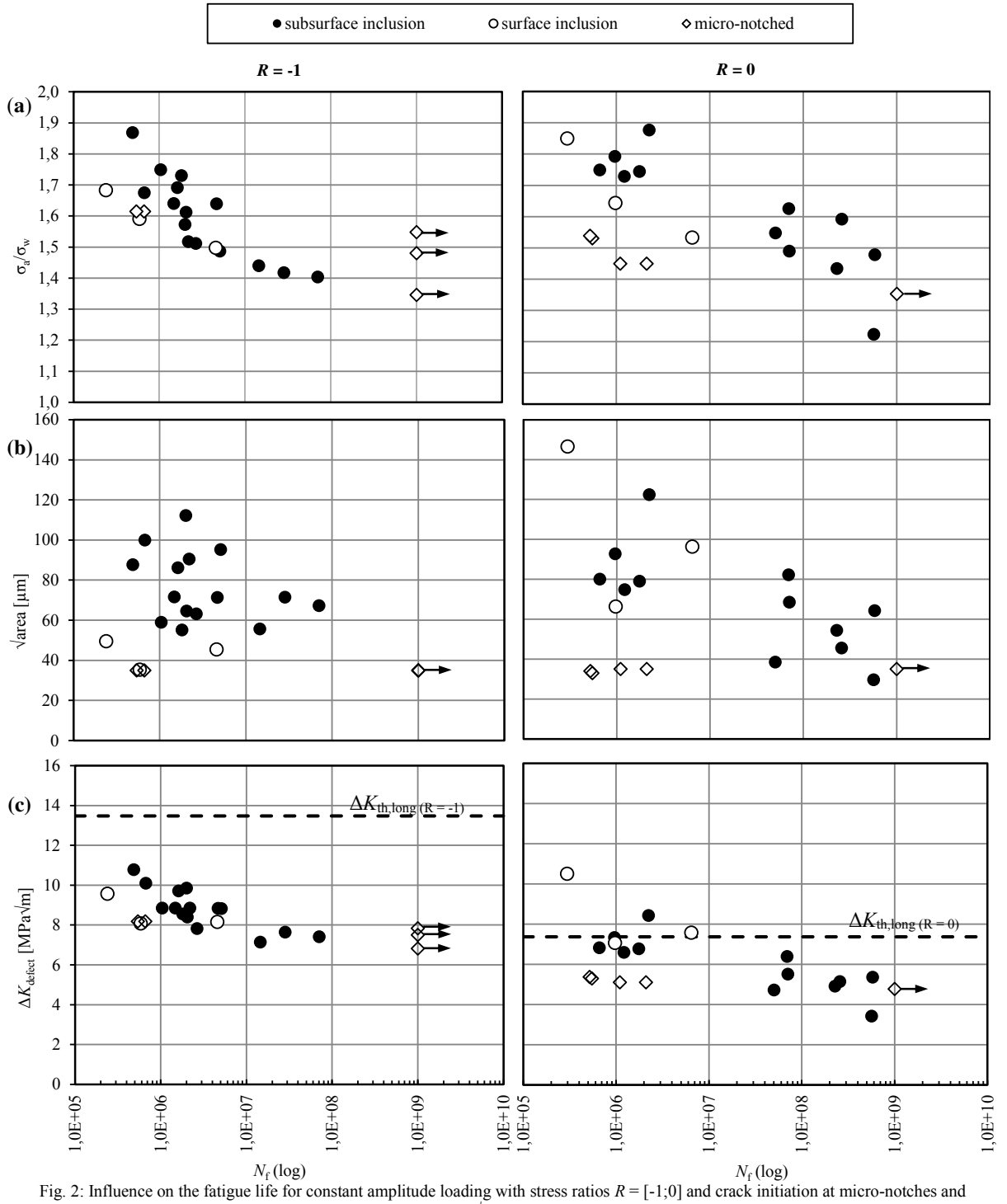

Fig. 2: Influence on the fatigue life for constant amplitude loading with stress ratios R = [-1;0] and crack initiation at micro-notches and inclusions: a) modified S-N curve , b) √area and c) cyclic stress intensity of the defect

The approach by *Fujimoto* results in $\Delta K_{defect}/\Delta K_{th}$ values greater than one for broken specimens and above one for run-outs, in case of both stress ratios. Thus, this approach yields the most accurate results. In contrary, the *Murakami*

approach underestimates even the calculated threshold value for the run-outs by a minimum factor of 1.34. For $R = 0$ the approach by *Murakami* yields acceptable results.

4.2. Fatigue behavior for variable amplitude loading

For the investigated load spectrum FELIX the results of SSI and micro-notches for $R = -1$ are shown in Figure 3. Both, SSI and micro-notches lead to fatigue failure in the VHCF regime.

For plotting the modified S-N curve the maximum stress amplitude $\bar{\sigma}_a$ of the load spectrum was used. For higher fatigue lives $N_f > 10^7$ the $\bar{\sigma}_a/\sigma_w$ values of the micro-notches are in the range of the SSI. However, for lower fatigue lives the defect sizes become more crucial, whereby the SSI size is much higher compared to the micro-notch size for the same fatigue life values. However, this discrepancy is decreasing with increasing fatigue life.

Using the linear damage accumulation an equivalent constant stress amplitude $\sigma_{a,eq}$ of the load spectrum FELIX has been calculated. Afterwards an equivalent stress intensity factor $\Delta K_{defect,eq}$ with equation (2) using $\Delta\sigma_{eq} = 2 \cdot \sigma_{a,eq}$ has been calculated. The results for SSI, are about $\Delta K_{defect,eq} = [6.0 – 11.0]$ MPa$\sqrt{m}$ and are in the range of CA tests (Figure 2). However, micro-notches lead to $\Delta K_{defect,eq} = [6.0 – 8.0]$ MPa$\sqrt{m}$ and therewith they are lower in comparison to CA tests with $\Delta K_{defect} > 8.0$ MPa$\sqrt{m}$.

In Figure 4b the S-N curves of the micro-notch tests for both R-ratios and of SSI tests for $R = -1$ are plotted. The micro-notch tests for $R = -1$ with the maximum stress amplitude of 705 MPa and 673 MPa lead to results within the scatter band of SSI results. The lowest $\bar{\sigma}_a$ value of 641 MPa results in fatigue failure in case of SSI, whereby specimens with micro-notches do not fail on this stress level. In case of $R = 0$, no SSI failure of smooth specimen occurred. However, for micro-notched specimen VHCF failure can be observed.

Because of the great amount of cycles of the load spectrum FELIX beneath the fatigue strength (see Table 1), the damaging effect of these low load amplitudes has to be evaluated. Therefore, linear damage accumulation calculations have been performed for the modified FELIX spectrum on the basis of CA data for smooth specimen. With the original *Palmgren-Miner* (PM) rule [12], only stress amplitudes above the fatigue strength contribute to damage. However, there exist a few modifications of the PM rule taking stress amplitudes beneath the fatigue strength into account. The elementary PM rule extends the S-N curve beneath the fatigue strength with a constant slope k. This approach often overestimates the fatigue strength, because the damaging effect corresponding to low stress amplitudes is too high. Whereby the modified PM rule [13] adapts the slope beneath the fatigue strength with $2k$-1. This modification considers a less high damaging effect of low stress amplitudes. Calculated Gassner lines with this three PM-rules for both R-ratios have been determined and compared to the experimental results, as shown in Figure 4b.

For $R = -1$ three different calculated Gassner lines are shown. The elementary PM-rule (solid line) underestimates the fatigue life of micro-notches and SSI tests. This difference becomes more crucial with increasing fatigue life, especially in the case of micro-notch tests. The original and modified PM-rule lead to nearly the same fatigue lives. Furthermore, the original rule leads to the highest fatigue lives. These two PM-rules are within the scatter band of the experimental results, but the slopes of the Gassner lines do not match the experimental results. Since the original and the modified PM-rule fit the experimental results – especially for lower $\bar{\sigma}_a$ values – better than the elementary PM-rule, the authors conclude that stress amplitudes beneath the fatigue strength do not equally or even do not at all contribute to damage such as stress amplitudes above the fatigue strength.

In the case of $R = 0$, the three PM-rules results in identical Gassner lines. One explanation for this result is the high slope $k = 37$ of the S-N curve corresponding to the CA data for smooth specimen, that is about 9.3 times higher than the slope of $R = -1$. Thus, the lower load amplitudes do not contribute to the linear damage accumulation, because the corresponding tolerable number of cycles is extremely high. Thus, the calculated Gassner line contains only the amount of damage corresponding to stress amplitudes above the fatigue strength and is equally to the original PM-rule. Since this Gassner line fits the experimental results of micro-notch tests in good agreement, the authors conclude, that only stress amplitudes above the fatigue strength contribute to damage in this case.

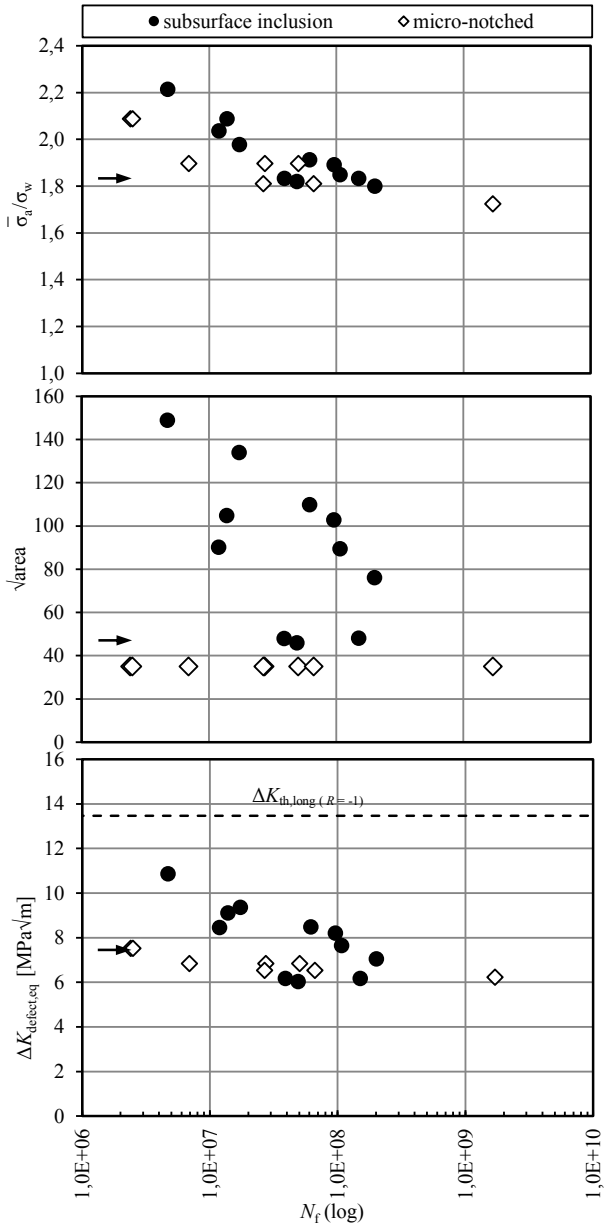

Fig. 3: Influence of defect size on the fatigue life for crack initiation at micro-notches and SSI, using modified S-N curve, √area and the cyclic stress intensity of the defect with R = -1 for VA loading

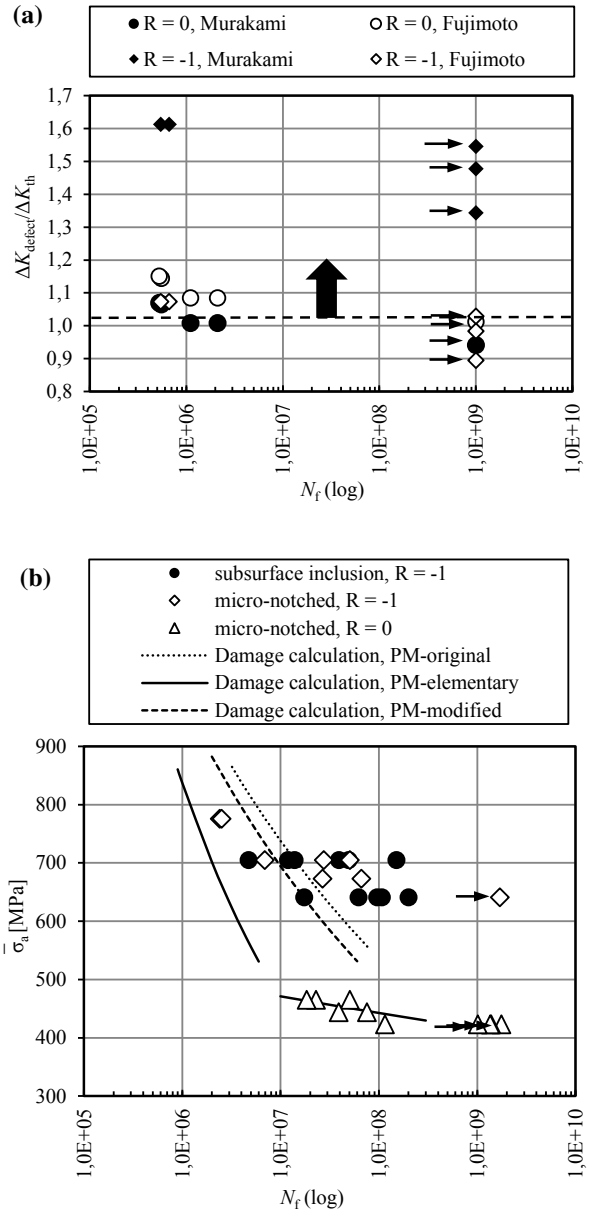

Fig. 4: Comparison of ΔK_{th} approaches with experimental CA - data (a) and comparison of S-N curves for VA- and CA-tests and calculated *Gassner* lines (b)

5. Conclusions

Fatigue tests with micro-notched specimens with two different *R*-ratios using an ultrasonic fatigue testing system has been performed and compared to previous investigations with smooth specimens. The micro-notches are introduced by a pico-second laser at the surface of smooth specimens at the center of the gauge length. Tests have

been done at constant amplitude (CA) loading and variable amplitude (VA) loading with a reconstructed load time history called FELIX. Following conclusions can be made for

a) CA-tests:
    1. As opposed to tests with smooth specimens, no VHCF-failure for micro-notch tests occurs.
    2. Surface inclusion sizes that lead to fatigue failure are in the range of the micro-notch for R = -1. However, in case of a stress ratio of 0, the surface inclusion has to be much larger to initiate a fatigue crack.
    3. The approach by *Fujimoto* et al. for the threshold stress intensity factor as function of the defect size gives the most appropriate conformity in comparison to the experimental results.

b) VA-tests:
    1. VHCF-failure ($N_f > 10^7$) for micro-notch tests occur for both R-ratios.
    2. Inclusion sizes are larger, compared to the size of the micro-notch, which lead to fatigue failure for R = -1.
    3. Comparing the calculated Gassner lines with the experimental results, the authors can conclude, that the damaging effect of amplitudes below the fatigue strength is low independent of the investigated R-ratio.

For future work, the influence of the size of the micro-notch will be investigated. In particular, the transition of the crack initiation site from surface to subsurface in terms of VA tests will be focused.

For a systematical investigation of load interaction effects in the VHCF regime, single overload tests will be performed. Moreover, the amount of crack propagation compared to the total fatigue life will be determined by evaluated arrest marks on the fracture surface.

Acknowledgment

The authors gratefully acknowledge the financial support by the DFG within the framework of the SPP 1466.

References

[1] Mayer, H.; Stochjanovic, S.; Ede, C.; Zettl, B.: Beitrag niedriger Lastamplituden zur Ermüdungsschädigung von 0,15 % C Stahl. In: Mat.-wiss. U. Werkstofftech., 38, 2007, pp. 581-590.
[2] Müller, T.; Sander, M.: On the use of ultrasonic fatigue testing technique – Variable amplitude loadings and crack growth monitoring. Ultrasonics, 53, 2013, pp. 1417-1424.
[3] Mayer, H.; Haydn, W; Schuller, R.; Issler, S.; Bacher-Höchst, M.: Very high cycle fatigue properties of bainitic high carbon-chronium steel under variable amplitude loading. In: IJF, Vol. 28, 2009, pp. 1300-1308.
[4] Sander, M.; Müller, T., Lebahn, J.: Influence of mean stress and variable amplitude loading on the fatigue behaviour of a high-strength steel in VHCF regime. Vol. 62, IJF, 2014, pp. 10-20.
[5] Müller, T.; Sander, M.: Experimental investigation and damage calculations of a load time history in the very high cycle fatigue. AMR, Vols. 891-892, 2014, pp. 446-451.
[6] Masaki, K.; Ochi, Y.; Matsumura, T.: Small crack property of austenitic stainless steel with artificial corrosion pit in long life regime of fatigue. In: International Journal of Fatigue 28 (11), pp. 1603–1610, 2006. DOI: 10.1016/j.ijfatigue.2005.06.055.
[7] Schönbauer, B.M.; Stanzl-Tschegg, S.; Perlega, A.; Salzman, R.N.; Rieger, N.F.; Zhou, S.; Turnbull, A.; Gandy, D.: Fatigue life estimation of pitted 12% Cr steam turbine blade steel in different enviroments and at different stress ratios. IJF, Vol. 65, 2014, pp. 33-4.3
[8] Beretta, S.; Carboni, M.; Fiore, G.; Lo Conte, A.: Corrosion–fatigue of A1N railway axle steel exposed to rainwater. In: International Journal of Fatigue 32 (6), 2010, S. 952–961.
[9] Edwards, P.R.; Darts, J.: Standardised fatigue loading sequences for helicopter rotors – Helix and Felix – Part 1: background and fatigue evaluation and Part 2: final definition of Helix and Felix. NLR TR 84043 U; 1984.
[10] Murakami, Y.: Metal fatigue: Effects of small defects and nonmetallic inclusions. Elsevier Science Ltd., 2002.
[11] Fujimoto, Y.; Hamada, K.; Shintaku, E.; Pirker, G.: Inherent damage zone model for strength valuation of small fatigue cracks. In: EFM, Vol. 68, 2001, pp. 455-473.
[12] Miner, M.A.: Cumulative damage in fatigue. J. Appl. Mech. 12 (1945), S. 159/64.
[13] Haibach, E.: Betriebsfestigkeit – Verfahren und Daten zur Bauteilberechnung. Springer-Verlag, Berlin Heidelberg, 2006